Evaluation of 5G NR Capacity in HAPS System

Dwi Harinitha[1*,2], Iskandar[1] and Irma Zakia[1]

[1]School of Electrical Engineering and Informatics, Institut Teknologi Bandung, Bandung, Indonesia [2]Department of Electrical Engineering, Institut Teknologi Padang, Padang, Indonesia
[*]33219006@std.stei.itb.ac.id

Abstract: High infrastructure costs and rugged terrain prevent rural and remote 5G mobile network deployment. High-altitude platform stations (HAPS) in the stratosphere offer line-of-sight connectivity and wide coverage, making them a promising non-terrestrial alternative to terrestrial base stations. With particular attention to important technical parameters, including numerology, bandwidth, antenna size, and modulation scheme, this work explores the system-level performance of HAPS-based 5G networks. A simulation-based approach was employed by 3GPP 5G new radio (NR) specifications to evaluate their impact on system capacity and the number of supported user equipment (UE). Results indicate that lower numerology, specifically 0, improves spectral efficiency and user capacity, while bandwidth expansion (30-45 MHz) boosts throughput. Due to faster resource saturation, larger antenna arrays improve data rates but reduce user capacity. In rural areas with poor channel conditions, higher-order modulation improves data rate but reduces system robustness. The findings suggest that optimal HAPS deployment in underserved regions should prioritize low numerology, moderate-to-large antenna configurations, bandwidth flexibility, and adaptive modulation (QPSK–64-QAM). These configurations enable reliable and scalable 5G services in areas without terrestrial infrastructure, making HAPS a key enabler for non-terrestrial networks (NTNs) integration in the global IMT-2020 framework. This research aids digital inclusion and 5G connectivity.

Keywords: 5G NR; data rate; HIBS; non-terrestrial network; numerology.

1. Introduction

Compared to past generations, the fifth generation (5G) of cellular communication technology has greatly improved spectral efficiency, network capacity, and data transmission rates [1]. Mass Internet of Things (IoT) installations, autonomous cars, and ultra-reliable low-latency communications are only a few of the many uses these developments have made possible [2]. Nevertheless, the deployment of 5G infrastructure is still uneven, especially in rural and remote areas, due to the great expenses and technical difficulties of installing terrestrial base stations in these areas [3]–[6].

High-altitude platform stations (HAPS) have become a promising fix for these constraints. Defined by the Radio Regulations (RR) No. 1.66A, HAPS are unmanned or manned aerial platforms flying in the stratosphere, usually at altitudes between 20 and 50 km [7], [8]. Practically, altitudes between 17 and 22 km are usually chosen because of rather stable atmospheric conditions and little disturbance of the temperature [9]. Current technical implementations of HAPS are embodied on platforms including Sunglider, Airbus Zephyr, Startobus, and Project Loon. HAPS have several operational benefits by using a special position between terrestrial and satellite infrastructure: wide-area coverage, high line-of-sight (LOS) communication probability, and lower ground infrastructure needs [8]. These features make HAPS a desirable enabler of 5G services in regions outside conventional networks. As such, HAPS are progressively seen as a fundamental component of non-terrestrial networks (NTNs) that enhance terrestrial 5G deployment strategies [10].

The function of HAPS in both standalone scenarios [11]–[14] and as part of integrated communication architectures [15]–[18] has lately been investigated. International regulatory and standardizing organizations have also formally recognized the value of HAPS. Reflecting

Received: March 5th, 2025. Accepted: June 15th, 2025
DOI: 10.15676/ijeei.2025.17.2.12

Resolution 221 of ITU-R M.2101, adopted during the 2023 World Radiocommunication Conference (WRC-23), the International Telecommunication Union (ITU) has included HAPS in its recommendations for International Mobile Telecommunications (IMT) services [19]. Moreover, the 3rd Generation Partnership Project (3GPP) has included HAPS in its technical specifications for NTNs, mostly in TR 38.811 [9], [20]–[23], which describes the technical parameters for 5G New Radio (NR) over HAPS.

Base stations (BS) in terrestrial mobile networks are made to be as many user equipment (UEs) as feasible while yet preserving the necessary data throughput and quality of service (QoS). In areas with difficult topography or low population density, however, network performance suffers greatly and sometimes results in intermittent or complete loss of connectivity [24]. This underlines the need for alternative infrastructure models and aggravates the digital divide separating urban and rural communities [10], [25]–[27]. Operating under IMT-designated frequency ranges, HAPS could be aerial base stations providing broadband connectivity over large areas. Nevertheless, due to the high-altitude nature of HAPS, detailed system-level performance analyses are required, particularly regarding system capacity and support for high data rates as mandated by 5G standards [28].

Several studies have addressed aspects of NTN deployment. For instance, [29] proposes power and location optimization strategies for UAV-based networks but focuses solely on single-user scenarios and does not address HAPS-specific configurations. Other works, such as [30], discuss 5G/6G NTN potential in remote areas but lack in-depth analysis of system capacity based on 5G-specific parameters like numerology and signaling overhead. Numerology in 5G plays a critical role in determining system performance, influencing spectral efficiency, interference sensitivity, and coverage range. Research such as [31] focuses on flexible HAPS payload architecture for high-speed 5G transmission but does not address system-level capacity modeling. A discussion on HAPS altitude optimization to enhance downlink communication performance has been conducted in the study [32]. Optimizing the altitude between 20 km and 26 km, achieving the maximum ergodic capacity at an altitude of 20 km. However, this study has not examined the influence of 5G numerology and variations in bandwidth. The authors in [33] proposed an approximation algorithm named Multi-BS, Multi-layer RB Allocation with Multicast (M^2RBAM) to solve the resource allocation problem. The developed algorithm significantly enhances the weighted sum ratio and user satisfaction ratio in multicast scenarios. Although it has focused on the Physical Resource Block (PRB) allocation algorithm, specifically vRB (virtual Resource Block) using mixed numerology, it has not touched on the numerology-based HAPS 5G performance model in the context of coverage area.

Meanwhile, studies in [34], [35] investigate capacity metrics for earlier technologies like 3G/CDMA and 4G/LTE, without exploring the implications of the latest 3GPP-compliant 5G NR specifications [36]. Notably, there remains a lack of comprehensive studies that examine the relationship between 5G numerology and HAPS system performance in terms of capacity, especially in rural contexts. Higher numerologies may enhance throughput but tend to be more susceptible to interference and reduced coverage (key challenges for HAPS-based communications). Therefore, this study aims to provide a quantitative analysis of how 5G numerology and other critical system parameters affect the capacity of HAPS-based communication systems within the 5G NR framework.

Based on the urgency to provide reliable and wide-reaching communication solutions in areas underserved by terrestrial networks, this study aims to quantitatively analyze the impact of key technical parameters, such as numerology, channel bandwidth, antenna size, and modulation schemes, on the capacity of 5G NR-based HAPS systems. Through a simulation approach that refers to the 3GPP technical specifications, this study evaluates how these configurations can be optimized to meet connectivity needs in rural and remote areas. For that reason, the structure of this study is organized into four main sections: Section I is the introduction that outlines the background and urgency of the topic; Section II explains in detail the HAPS system model used as the basis for the simulation; Section III presents the

simulation results and system performance analysis based on parameter variations; and Section IV concludes the main findings and provides technical recommendations for the implementation of HAPS as an IMT base station in geographically challenging environments.

2. System Model

The proposed system architecture is illustrated in Figure 1, where a HAPS operates at an altitude of approximately 20 km, enabling wide-area coverage beneath its footprint. To evaluate the system's theoretical capacity, the analysis begins with the classical Shannon capacity formula, defined in (1):

$$C = W \cdot n \cdot \log_2(1 + S/N) \quad (1)$$

in which C is the channel capacity (bps), W is the channel bandwidth (Hz), n denotes the number of antenna elements in the array (or sectors), and S/N is the signal-to-noise ratio (SNR). While this formulation provides a fundamental understanding of capacity under ideal conditions, it does not account for interference, which becomes critical in practical multi-user, multi-cell 5G environments.

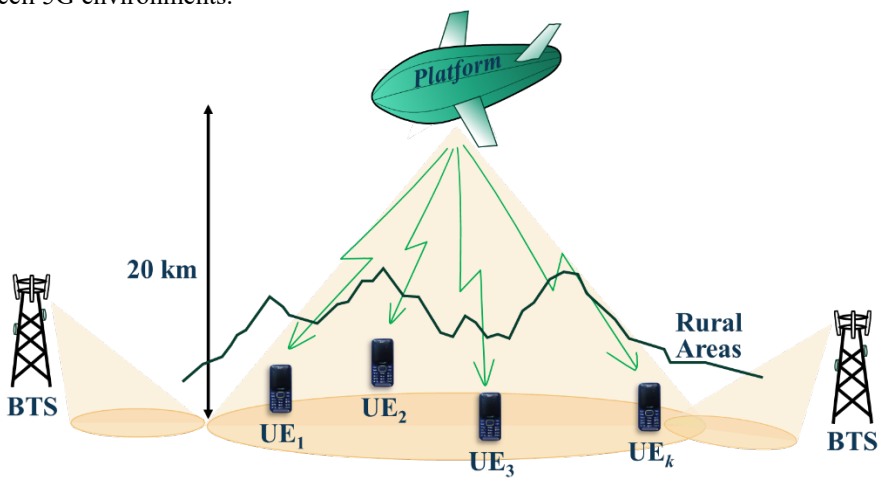

Figure 1. Topology of the system

To address this limitation, the analysis introduces the Signal-to-Interference-plus-Noise Ratio (SINR), which replaces SNR to accommodate interference effects. The general SINR is expressed as:

$$SINR = \frac{S}{I+N} \quad (2)$$

In multiuser systems, the SINR experienced by the k-th UE can be more accurately represented by:

$$SINR_k = \frac{g_k p_k}{\sum_{l \neq k} g_l p_l + n_k} \quad (3)$$

in which p_k is the transmit power of the k-th UE, g_k denotes the channel gain between the k-th UE and the receiver, and n_k is the additive white Gaussian noise (AWGN) power. The denominator represents the sum of interference power from other users and thermal noise, reflecting a more realistic propagation environment.

Furthermore, a thorough investigation is necessary to determine the system throughput and the role of 5G numerology. It is essential to emphasize that numerology, represented by the parameter μ, is a term used in wireless communication systems, such as 5G. Generally, numerology can be expressed as data transmission through the air in the form of carrier frequencies (carriers) divided into small parts (subcarriers). The subcarrier distance is regulated to determine the desired level of closeness or separation, which may affect the system's capacity and performance. Technically, as defined by the 3GPP 5G NR standard, the term

numerology refers to specific subcarrier spacing (SCS) configurations in the orthogonal frequency division multiplexing (OFDM) system. Therefore, a more detailed throughput estimation is conducted based on the 3GPP standard TS 38.306 v18.4.0 (2025-01), given in:

$$R = 10^{-6} \cdot \sum_{j=1}^{J} \left(v_{Layers}^{(j)} \cdot Q_m^{(j)} \cdot f^{(j)} R_{max} N_{PRB} \left(1 - OH^{(j)}\right) \right) \quad (4)$$

Here, R is the data rate in Mbps, and J is the number of aggregated component carriers (CCs). The parameters are defined as follows:

- $v_{Layers}^{(j)}$: maximum number of MIMO layers for the j-th CC.
- $Q_m^{(j)}$: modulation order for the j-th CC.
- $f^{(j)}$: scaling factor (values: 0.4, 0.75, 0.8, or 1).
- R_{max}: maximum code rate, as specified in 3GPP TS 38.214 v17.13.0 (2025-04).
- N_{PRB}: physical resource blocks (PRBs), derived from:

$$N_{PRB} = \frac{N_{RB}^{BW(j)\cdot\mu} \cdot 12}{T_s^{\mu}} \quad (5)$$

in which μ is the numerology index defined in 3GPP TS 38.211 v18.6.0 (2025-04), and $BW^{(j)}$ is the maximum bandwidth supported by the UE in the specified band or band combination. The term $N_{RB}^{BW(j)\cdot\mu}$ is the maximum RB allocation as defined in 3GPP TS38.101-1 v18.8.0 (2025-02), TS38.101-2 v18.9.0 (2025-04), TS38.101-5 v18.9.0 (2025-04), and TS38.104 v18.9.0 (2025-04). The average OFDM symbol duration T_s^{μ}, assuming a normal cyclic prefix, is calculated as:

$$T_s^{\mu} = \frac{10^{-3}}{14 \cdot 2^{\mu}} \quad (6)$$

The control overhead term $OH^{(j)}$ accounts for signaling and varies based on frequency range and link direction:

- 0.14: Downlink (FR1)
- 0.18: Downlink (FR2)
- 0.08: Uplink (FR1)
- 0.10: Uplink (FR2)

In this study, the focus is placed on evaluating the achievable throughput in the downlink transmission. Evaluation by applying (4) under various system configurations, including different numerology values, antenna array sizes, modulation orders, and channel bandwidths. Analysis of SINR incorporating interference modeling, channel variation, and power allocation will be addressed in future extensions of this research.

3. Simulation Modeling

In pursuit of enhancing connectivity for rural and remote areas, this research evaluates the performance of a fifth-generation (5G) communication system facilitated by a HAPS operating at an altitude of 20 kilometers. The system operates at 2 GHz in downlink transmission, as defined in Resolution 221 WRC-23. Whereas the UE is presumed to employ a single antenna, the antenna on the HAPS is modeled as a uniform planar array (UPA). Setting the minimum elevation angle between HAPS and UE at 10 degrees helps to preserve LOS connectivity.

The influence of various important technical parameters on system capacity, notably numerology, channel bandwidth, array antenna size, and modulation scheme, was investigated by means of the simulation. Among the fixed parameter values in the simulation are one component carrier (j=1), a scaling factor of 1, and a control channel overhead set at 0.14 for downlink on Frequency Range 1 (FR1). Assume one UE needs a minimum allotment of two Physical Resource Blocks (PRB), hence the data rate threshold (R_{th}) is set at 1 Gbps. Digital modulation such as QPSK, 16-QAM, 64-QAM, and 256-QAM are among the scenario variants, including UPA antennas with 4×4, 8×8, and 16×16 elements. The channel bandwidth

is thus changed to the IMT spectrum in FR1, namely 10 MHz, 20 MHz, 30 MHz, and 45 MHz. Whereas the variation in bandwidth and numerology influences the maximum allocation of RB (N_{RB}), the variation in modulation techniques influences the goal code rate (R_{max}). According to the specifications of 3GPP TS 38.211, supported transmission numerologies for 5G systems can be stated in Table 1.

Table 1. Supported Transmission Numerologies for 5G Systems

Numerology (μ)	Subcarrier Spacing (SCS) $\Delta f = 2\mu \cdot 15$ [kHz]	Bandwidth per RB [kHz]
0	15	180
1	30	360
2	60	720
3	120	1440
4	240	2880
5	480	5760
6	960	11520

Simulations will also be conducted to see the system's bit error rate (BER) quality in data transmission. The planned environment is a rural or remote area with a Rician channel representing the dominant LOS propagation conditions in the HAPS communication system. The overall simulation parameters are summarized in Table 2.

Table 2. Simulation Parameters

Notation	Definition	Value
θ	Elevation angle	10°
μ	Numerology	0, 1, 2
B_{ch}	Bandwidth	10, 20, 30, 45 MHz
f	Operating frequency	2 GHz
h	Altitude of HAPS	20 km
J	The number of aggregated component carriers (CCs)	1
K	K-factor for Rician fading	10 dB
OH	Overhead	0.14
P_{tx}	Transmit power	43 dBm
Q_m	The modulation orders in digital modulation: QPSK, 16-QAM, 64-QAM, and 256-QAM	2, 4, 6, 8
R_{th}	Data rate threshold	1 Gbps
v_{Layers}	Maximum number of MIMO layers for the j-th CC: 4×4, 8×8, and 16×16 elements	4, 8,16

4. Results and Discussion

At the initial step, the simulation concentrated on observing the impact of numerology modifications on system capacity. In this instance, the HAPS antenna is configured as 4×4, with QPSK modulation, a bandwidth of 45 MHz, and R_{max} of 602 (on a scale of 1024). Based on the specifications of 3GPP TS 38.104 and the standards in Table 1, the theoretical values of N_{RB} for numerologies μ=0 to μ=6 are 250, 125, 62, 31, 15, 7, and 3, respectively. However, to ensure conformity with the 3GPP TS 38.204 technical requirements and considering the allotment of guard bands and alignment with raster channels, only numerologies μ=0, μ=1, and μ=2 are employed in the simulation. Each yields a maximum N_{RB} value of 242, 119, and 58, respectively. It is evident that the rise in numerology produces a decrease in the number of RBs that can be allocated. This immediately affects the number of UEs that may be supplied

simultaneously, as well as limiting the total system capacity. Therefore, a simulation was performed for the same RB allocation conditions to see the increase in system capacity with increasing numerology**.**

The simulation results in Figure 2 and Table 3 show that with a specific RB allocation, increasing numerology provides an increase in capacity. This is because of the larger subcarrier spacing at higher numerology, so the allocation of RB per unit bandwidth (spectrum efficiency) also increases. However, the duration of the symbol will be shorter, which will reduce the coverage range and give a significant delay effect. Thus, low numerology is likely suitable for wide coverage and areas with considerable channel delay. In contrast, high numerology is suitable for covering small or dense environments, and its delay requirements are also minor. Taking the ITU-T IMT-2020, the average user data rate for downlink is targeted at 100 Mbps, and this threshold has been met for the lowest numerology (μ=0) in the simulation. The decrease in data rate due to the change in numerology is moderate, but fairly important when regarded in the context of spectral efficiency and the achievability of the service threshold. In the HAPS implementation plan for rural areas, coverage is prioritized over data rate because the UE density is typically lower. Therefore, the μ=0 numerology was chosen as the optimal configuration for the following simulation scenario because it provides the best balance between capacity and service coverage range.

Table 3. System Throughput for Different Numerologies (μ)

Numerology (μ)	Data Rate [Mbps]
0	135.9
1	271.8
2	543.6

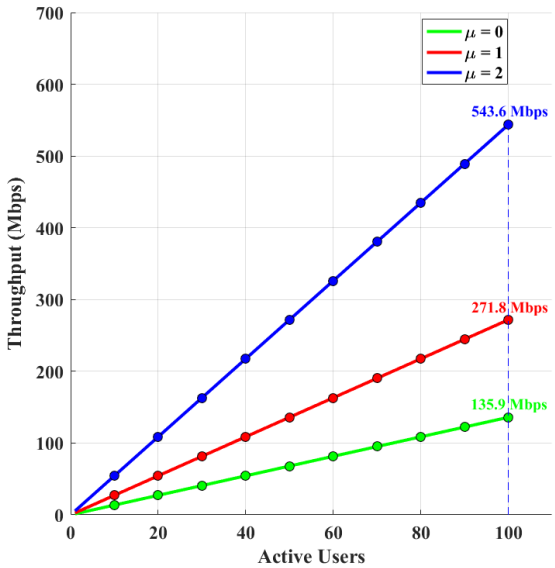

Figure 2. System throughput for different numerologies (μ)

The second simulation was done to analyze the influence of bandwidth variation on system capacity and the number of users that can be simultaneously serviced by HAPS. In this scenario, the parameters utilized as the basis for the simulation are a 4×4 UPA antenna size, a QPSK modulation scheme with a target coding rate of 602 (on a scale of 1024), and a fixed numerology at μ=0. The channel bandwidth varies four primary values, namely 10 MHz, 20 MHz, 30 MHz, and 45 MHz, which are part of the IMT spectrum for FR1.

Based on the 3GPP TS 38.104 standards [37], the maximum N_{RB} value for each bandwidth is as follows: 52 RB for 10 MHz, 106 RB for 20 MHz, 160 RB for 30 MHz, and 242 RB for 45 MHz. Unlike the influence of numerology, which demonstrates that the maximum resource block (N_{RB}) value drops with a rise in μ, simulation results (Table 4) reveal that increasing bandwidth actually raises the maximum N_{RB} value. With the increasing value of N_{RB}, the number of PRB that may be allocated to users also grows, which directly contributes to the increase in the number of UE that can be served in one transmission cycle. Hence, a wide bandwidth leads to more subcarriers or RBs being allocated, thereby increasing the system capacity, both in terms of the number of users (UEs) and the data rate.

Figure 3 depicts the simulation findings, showing a linear growing trend between bandwidth width and the maximum number of UEs that may be serviced. This linearity is realized due to the proportionality between the available bandwidth and RB. It demonstrates that the allocation of channel resources in the form of RB is heavily dependent on the availability of bandwidth. In addition, the increase in bandwidth also effects the potential data rate of the system, which is vital to address the high-speed communication needs in remote areas.

Table 4. System Throughput for Different Bandwidth

Bandwidth [MHz]	UE_{max}	Data Rate [Mbps]
10	26	35.3
20	53	72.0
30	80	108.7
45	121	164.4

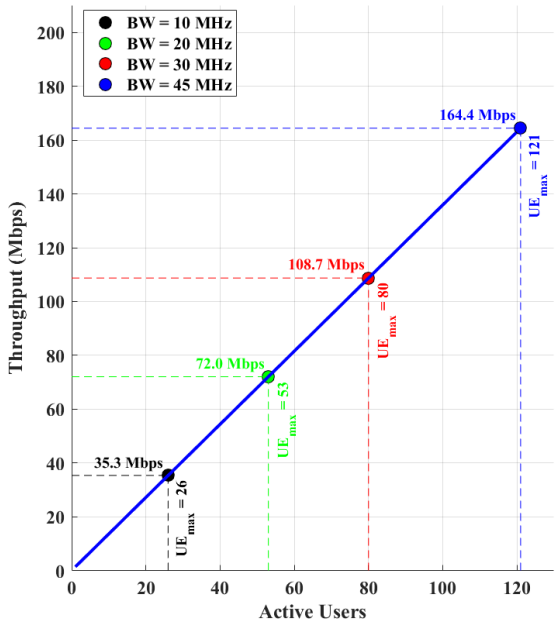

Figure 3. System throughput for different bandwidth

Drawing on the findings of this examination, a 45 MHz bandwidth was chosen as the ideal configuration for subsequent simulations. This pick is based on its capacity to supply the maximum number of RBs (242 RB), hence supporting a wider service coverage and a greater number of UEs in the HAPS network. Just like in the numerology variation scenario, changes

in the bandwidth parameter alter the value of N_{PRB} in the capacity equation (Equation (4)), which is the major indicator of the overall system performance.

The third simulation attempts to analyze the impact of antenna size variation on system capacity and the number of UE that can be served by HAPS. In this context, the antenna size is directly linked to the number of spatial layers supported (v_{Layers}), in accordance with the principles of MIMO (Multiple-Input Multiple-Output) processing. The three antenna designs employed in this simulation are UPA sized 4×4, 8×8, and 16×16, each assumed to support 4, 8, and 16 layers, respectively.

The simulation findings in Table 5 and Figure 4 demonstrate that increasing the antenna size leads to a significant improvement in the data rate. It is affected by the increase in antenna size, which allows for higher spatial multiplexing in order to realize simultaneous transmission of data streams to different UEs. Effectively, this procedure increases the overall system throughput. The data rate figures obtained are 164.4 Mbps for the 4×4 antenna, 328.9 Mbps for the 8×8, and 657.8 Mbps for the 16×16. These three configurations have exceeded the minimum capacity requirements of the IMT-2020 network as outlined in the ITU-R M.2083-0 document, which states that future communication systems must be able to support a data rate per user of up to 100 Mbps for enhanced mobile broadband (eMBB) applications.

Table 5. System Throughput for Different Antenna Sizes

Antenna	v_{Layers}	Data Rate [Mbps]
4×4	4	164.4
8×8	8	328.9
16×16	16	657.8

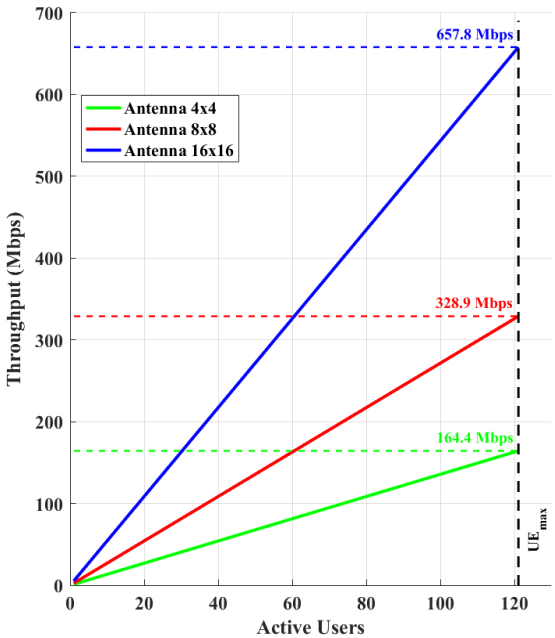

Figure 4. System throughput for different antenna sizes

Although increasing the antenna size enhances the overall system throughput, an intriguing phenomenon was identified regarding the number of UEs that may be supplied until attaining the established data rate threshold (R_{th}), which is 1 Gbps. Based on Table 6 and Figure 5, the increase in antenna size actually limits the number of UEs that can be served simultaneously.

This arises because the data rate per user increases dramatically, hence the resource block (RB) need for each UE gets larger. In other words, the bigger the individual UE capacity, the sooner the system resources reach the service threshold (R_{th}), which eventually restricts the total number of active users that may be handled simultaneously.

These data show a trade-off between greater throughput and multiuser efficiency. Therefore, establishing the antenna layout in HAPS implementation not only depends on the effort to optimize system capacity but also needs to consider the efficiency of resource allocation in user-dense scenarios. This becomes crucial in the context of HAPS networks meant for rural areas, where optimizing the number of users that may be serviced simultaneously is one of the key concerns.

Table 6. Active Users at 1 Gbps Throughput for Different Antenna Sizes

Antenna	v_{Layers}	UE_{max}
4×4	4	736
8×8	8	368
16×16	16	184

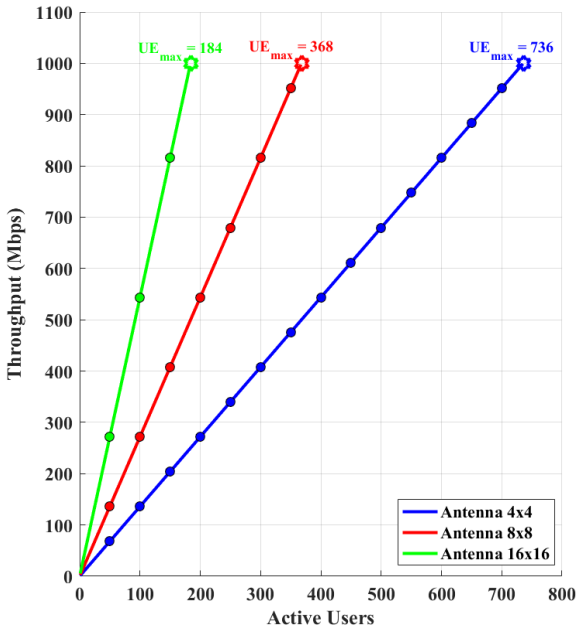

Figure 5. Active users at 1 Gbps throughput for different antenna sizes

Finally, variations were made to observe the effect of modulation, resulting in differences in the modulation order (Q_m), which also caused differences in the target code rate. As with the variation in antenna size, in different modulations, when Q_m increases, the data rate also increases, namely 164.4 Mbps for QPSK modulation, 359.5 Mbps for 16-QAM, 776.9 Mbps for 64-QAM, and 1035.8 Mbps for 256-QAM. The effect can be seen directly in Table 7 and Figure 6. This condition occurs because, at higher modulation orders, the number of bits per encoded symbol increases, resulting in enhanced spectral efficiency and throughput. However, this modulation scheme will require a higher SNR to maintain an acceptable bit error rate for communication feasibility. A supplementary simulation will be performed to demonstrate this requirement. Moreover, when the data rate threshold is reapplied at 1 Gbps when the modulation order increases, the number of served UEs remains small, but the system threshold has been reached. It can be seen in Table 8 and Figure 7 that in QPSK modulation, the number

of UEs that can still be served is 736 UEs, while in 256-QAM, only 117 UEs can be served because when serving that number of UEs, the system has already reached the threshold. This trade-off arises when the modulation order increases. Consequently, more RBs per UE are required to achieve higher data rates. As a result, faster resource consumption causes the system to reach its total RB capacity with fewer UE devices.

Table 7. System Throughput for Different Modulation Types

Modulation	Q_m	Data Rate [Mbps]
QPSK	2	164.4
16-QAM	4	359.5
64-QAM	6	776.9
256-QAM	8	1035.8

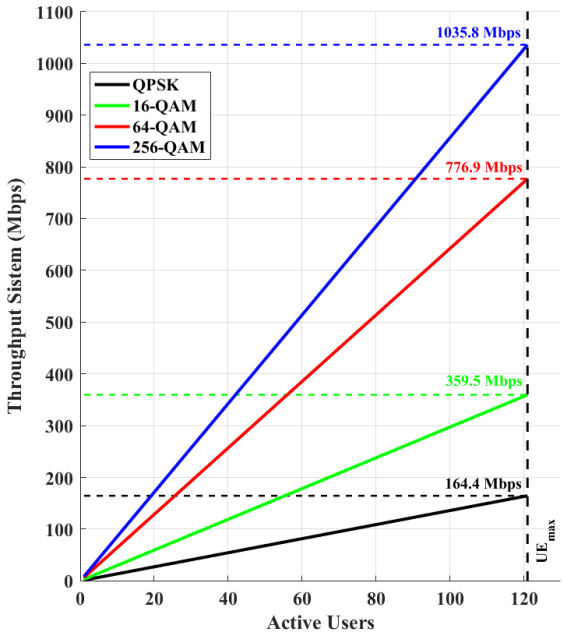

Figure 6. System throughput for different modulation types

From the simulations conducted with four modifications of parameters, it can be said that the numerology determines the data rate obtained; consequently, the numerology decides the smaller the UEs that can be provided. Stated simply, a change in numerology directly related to the data rate but inversely proportional to the number of UEs that might be supplied. Variations in bandwidth directly affect data rate and the number of UEs; hence, they directly correlate. Both changes in antenna size and modulation completely match the data rate. Conversely, when one desires to exceed the data rate threshold, the condition is inversely proportional to the number of UEs. With the situation of UE positions being far apart in rural or isolated places, the purpose is for communication to remain covered. The communication system should be able to cover a vast region, distribute UEs, offer consistent modulation for instances when the channel occasionally breaks, and give a suitable rate. One can select a low numerology (μ=0) for this circumstance. Then utilize extra antennas, 8×8 or 16×16, which can deliver better and more constant coverage. This will also enable the UE to precisely receive the signal, therefore enhancing the ability of the system to operate. Since the antenna size is already relatively large, QPSK can be selected for modulation with a maximum of 64-QAM to meet declining channel conditions. With QPSK, even if the data speed would be poor, it may

overcome bad signal quality in rural or remote places and offer a larger range, so facilitating a steady connection. One can choose 30 MHz or 45 MHz for bandwidth, which can be modified depending on local restrictions.

Table 8. Active Users at 1 Gbps Throughput for Different Modulation Types

Modulation	Q_m	Data Rate [Mbps]
QPSK	2	736
16-QAM	4	337
64-QAM	6	156
256-QAM	8	117

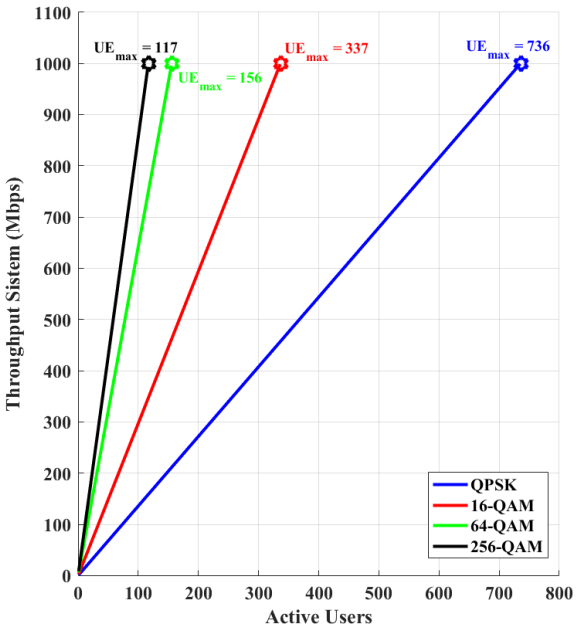

Figure 7. Active users at 1 Gbps throughput for different modulation types

Figure 8 describes the system in terms of bit error rate (BER), which incorporates the SNR discussed previously. The simulation was carried out for a rural environment with a Rician channel with numerology and modulation variations. The simulation results for numerology variations $\mu = 0$, 1, and 2 are shown in Figure 8a. It can be seen that the higher the numerology, the BER value also increases in the same SNR range. Increased numerology necessitates greater subcarrier spacing and reduced symbol duration. This condition renders the system more vulnerable to inter-symbol interference while diminishing tolerance to delay spread, particularly in multipath situations. The result indicates that communication has become increasingly unreliable. Therefore, in the modulation variation (Figure 8b), the selected numerology is fixed at $\mu = 0$. Furthermore, it can be seen that increasing the modulation order can increase the maximum data rate. However, it significantly worsens the BER performance, especially at low SNR, which indicates greater sensitivity to channel degradation. Higher-order modulations utilize denser symbol constellations, thereby increasing the possibility of symbol errors and leading to a higher BER at low SNR levels. Based on this, to maintain communication stability in rural environments with fluctuating channels, the recommended numerology is $\mu = 0$. Meanwhile, the modulation scheme selection should be adjusted to the throughput requirements and link conditions or channel quality. QPSK is very suitable for use in poor channel conditions because it is more noise-resistant. In contrast, 64-QAM modulation

can be used in better channel conditions with high data rate requirements, but only if the system supports adaptive modulation. Thus, the system can automatically switch to QPSK modulation to maintain communication when channel conditions deteriorate.

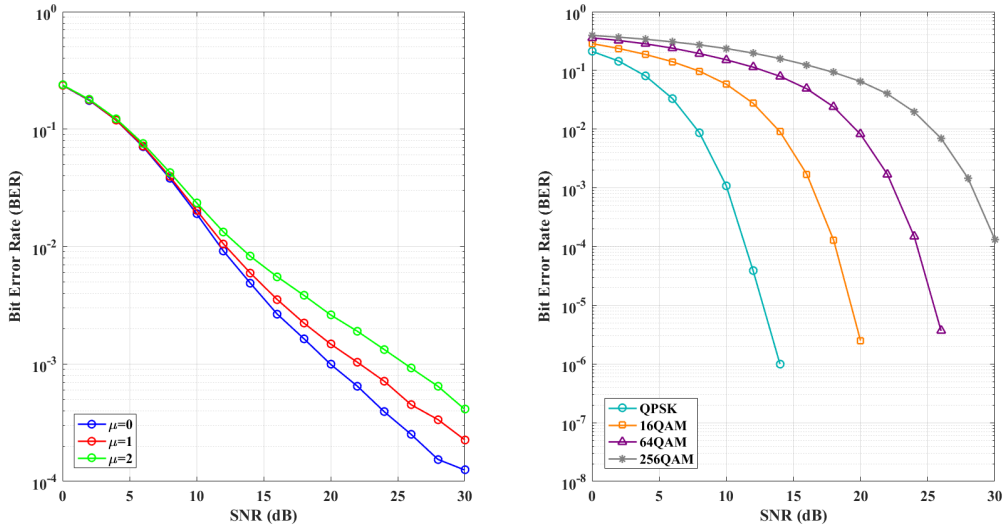

(a) (b)

Figure 8. BER vs SNR expressed with variations: (a) numerology and (b) modulation.

5. Conclusions

This paper shows how feasible High-altitude platform stations (HAPS) are as aerial base stations for 5G coverage in underdeveloped and rural areas. The study assessed numerology, bandwidth, antenna array size, modulation impact system capacity, and user support using system-level simulations matched with 3GPP 5G NR specifications. The results show that for higher capacity, a bandwidth of 30 MHz or 45 MHz is used. For numerology, the lower one (μ=0) offers better spectral efficiency and a wider user range. While larger antenna arrays (e.g., 8×8 and 16×16) improve data rates via spatial multiplexing, they also speed resource consumption, so limiting the number of concurrent users. Higher-order modulations such as 256-QAM similarly increase capacity but are less dependable under the variable channel conditions common in rural areas. Thus, to guarantee strong and efficient HAPS-based 5G deployment, a configuration combining low numerology, adaptive modulation (preferably QPSK to 64-QAM), moderate-to-large antenna arrays, and high bandwidth is advised. These revelations help to strategically integrate HAPS into non-terrestrial networks (NTNs), in line with world IMT-2020 targets, and provide a scalable solution to close the digital divide in geographically demanding areas.

6. Acknowledgment

This work was supported in part by the National Research and Innovation Agency (BRIN).

7. References

[1] K. Shah, "Advancements in 5G Technology : Challenges and Opportunities for Nationwide Deployment," *J. Artif. Intell. Cloud Comput.*, vol. 1, no. 3, pp. 1–9, 2022.

[2] G. A. Sampedro, S. L. Huyo-A, R. G. Kim, Y. J. Aruan, and M. Abisado, "Application of 5G Infrastructure for IoT: Challenges and Opportunities," *Proc. - 2022 2nd Int. Conf. Electron. Electr. Eng. Intell. Syst. ICE3IS 2022*, no. November, pp. 153–157, 2022, doi: 10.1109/ICE3IS56585.2022.10010238.

[3] S. K. A. Kumar and E. J. Oughton, “Infrastructure Sharing Strategies for Wireless Broadband,” *IEEE Commun. Mag.*, vol. 61, no. 7, pp. 46–52, 2023, doi: 10.1109/MCOM.005.2200698.

[4] I. A. Gedel and N. I. Nwulu, “Infrastructure Sharing for 5G Deployment: A Techno-Economic Analysis,” *Int. J. Interact. Mob. Technol.*, vol. 15, no. 2, pp. 137–156, 2021, doi: 10.3991/ijim.v15i02.16749.

[5] H. Maluleke, A. Bagula, O. Ajayi, and L. Chiaraviglio, “An Economic Feasibility Model for Sustainable 5G Networks in Rural Dwellings of South Africa,” *Sustain.*, vol. 14, no. 19, pp. 1–24, 2022, doi: 10.3390/su141912153.

[6] A. M. Cavalcante, M. V. Marquezini, L. Mendes, and C. S. Moreno, “5G for Remote Areas: Challenges, Opportunities and Business Modeling for Brazil,” *IEEE Access*, vol. 9, pp. 10829–10843, 2021, doi: 10.1109/ACCESS.2021.3050742.

[7] O. Abbasi, A. Yadav, H. Yanikomeroglu, N. D. Dào, G. Senarath, and P. Zhu, “HAPS for 6G Networks: Potential Use Cases, Open Challenges, and Possible Solutions,” *IEEE Wirel. Commun.*, vol. 31, no. 3, pp. 324–331, 2024, doi: 10.1109/MWC.012.2200365.

[8] Y. Hmamouche, M. Benjillali, and S. Saoudi, “Terrestrial Connectivity Through Constellations of High Altitude Platform Station (HAPS),” *11th Int. Symp. Signal, Image, Video Commun. ISIVC 2022 - Conf. Proc.*, pp. 1–6, 2022, doi: 10.1109/ISIVC54825.2022.9800720.

[9] Z. Lou, B. E. Youcef Belmekki, and M. S. Alouini, “HAPS in the Non-Terrestrial Network Nexus: Prospective Architectures and Performance Insights,” *IEEE Wirel. Commun.*, vol. 30, no. 6, pp. 52–58, 2023, doi: 10.1109/MWC.004.2300198.

[10] S. Stellatou and C. Erotokritou, “High-Altitude Platform Stations (HAPS); Regulatory Obstacles Blocking Their Deployment,” *2024 Int. Conf. Unmanned Aircr. Syst. ICUAS 2024*, pp. 363–369, 2024, doi: 10.1109/ICUAS60882.2024.10556966.

[11] A. A. Abu-Arabia, I. Iskandar, and R. Hakimi, “Performance of 5G Services Deployed via HAPS System,” in *2019 IEEE 13th International Conference on Telecommunication Systems, Services, and Applications (TSSA)*, 2019, pp. 168–172.

[12] F. A. D’Oliveira, F. C. L. De Melo, and T. C. Devezas, “High-altitude platforms — Present situation and technology trends,” *J. Aerosp. Technol. Manag.*, vol. 8, no. 3, pp. 249–262, 2016, doi: 10.5028/jatm.v8i3.699.

[13] A.-M. Hasan and M. Islam, “Improving the System Performance of High Altitude Platforms Serving Suburban Areas,” Blekinge Institute of Technology School, 2012.

[14] S. Karapantazis and F. N. Pavlidou, “Broadband communications via high-altitude platforms: A survey,” *IEEE Commun. Surv. Tutorials*, vol. 7, no. 1, pp. 2–31, 2005, doi: 10.1109/COMST.2005.1423332.

[15] G. Giambene, E. O. Addo, Q. Chen, and S. Kota, “Design and Analysis of Low-Power IoT in Remote Areas with NTN Opportunistic Connectivity,” *IEEE Trans. Aerosp. Electron. Syst.*, vol. 61, no. 2, pp. 2309–2328, 2025, doi: 10.1109/TAES.2024.3471991.

[16] S. Shang, E. Zedini, and M. S. Alouini, “Enhancing Non-Terrestrial Network Performance with Free Space Optical Links and Intelligent Reflecting Surfaces,” *IEEE Trans. Wirel. Commun.*, vol. 24, no. 2, pp. 1046–1059, 2025, doi: 10.1109/TWC.2024.3504359.

[17] M. Konishi, T. Nishimaki, Y. Shibata, S. Nabatame, and A. Nagate, “A Study of Co-Channel Spectrum-Sharing System between HAPS and Terrestrial Mobile Communication Networks,” in *2020 IEEE 91st Vehicular Technology Conference (VTC2020-Spring)*, 2020, pp. 1–5.

[18] S. Gharbi, N. Zangar, and N. Aitsaadi, “Overview: High Altitude Platform Network for Disaster and Crises Application,” *6th Int. Conf. Inf. Commun. Technol. Disaster Manag. ICT-DM 2019*, pp. 2019–2020, 2019, doi: 10.1109/ICT-DM47966.2019.9032991.

[19] Y. Zhou, F. Qi, and W. Xie, “Research on Spectrum Needs Prediction Method for HAPS as IMT Base Station,” *IEEE Access*, vol. 10, no. October, pp. 119095–119105, 2022, doi: 10.1109/ACCESS.2022.3220839.

[20] G. B. Koc, B. Ciloglu, M. Ozturk, and H. Yanikomeroglu, "HAPS-Enabled Sustainability Provision in Cellular Networks Through Cell-Switching," *2023 IEEE Int. Black Sea Conf. Commun. Networking, BlackSeaCom 2023*, pp. 294–299, 2023, doi: 10.1109/BlackSeaCom58138.2023.10299797.
[21] Y. Liu, R. Zhang, and Y. Zhou, "Challenges and Status of 3GPP Non-Terrestrial Networks for Mobile Terminal Testing," *ICMMT - Int. Conf. Microw. Millim. Wave Technol.*, vol. 1, no. 2024, pp. 1–3, 2024, doi: 10.1109/ICMMT61774.2024.10671764.
[22] Z. Zhang, H. Guo, and W. Xie, "Research of NTN Technical Scheme Based on 5G Network," *IEEE Int. Symp. Broadband Multimed. Syst. Broadcast. BMSB*, vol. 2023-June, pp. 1–6, 2023, doi: 10.1109/BMSB58369.2023.10211164.
[23] Y. Zhou and J. Wang, "MIMO-assisted HAPS as IMT Base Station for Downlink Spectrum Efficiency Enhancement," *2023 Int. Wirel. Commun. Mob. Comput. IWCMC 2023*, pp. 87–92, 2023, doi: 10.1109/IWCMC58020.2023.10182862.
[24] L. Feltrin, N. Jaldén, E. Trojer, and G. Wikström, "Potential for Deep Rural Broadband Coverage With Terrestrial and Non-Terrestrial Radio Networks," *Front. Commun. Networks*, vol. 2, no. July, pp. 1–11, 2021, doi: 10.3389/frcmn.2021.691625.
[25] H. M. Hussien, K. Katzis, L. P. Mfupe, and E. T. Bekele, "Bridging the Urban-Rural Broadband Connectivity Gap using 5G Enabled HAPs Communication Exploiting TVWS Spectrum," *J. Eng. Res. Sci.*, vol. 1, no. 2, pp. 24–32, 2022, doi: 10.55708/js0102003.
[26] S. Alfattani, W. Jaafar, H. Yanikomeroglu, and A. Yongaçoglu, "Multi-Mode High Altitude Platform Stations (HAPS) for Next Generation Wireless Networks," pp. 1–7, 2022.
[27] J. P. R. Pereira, "Broadband access and digital divide," *Adv. Intell. Syst. Comput.*, vol. 445, pp. 363–368, 2016, doi: 10.1007/978-3-319-31307-8_38.
[28] S. Euler, X. Lin, E. Tejedor, and E. Obregon, "High-Altitude Platform Stations as International Mobile Telecommunications Base Stations: A Primer on HIBS," *IEEE Veh. Technol. Mag.*, vol. 17, no. 4, pp. 92–100, 2022, doi: 10.1109/MVT.2022.3202004.
[29] L. Zhu, J. Zhang, Z. Xiao, X. Cao, X. G. Xia, and R. Schober, "Millimeter-Wave Full-Duplex UAV Relay: Joint Positioning, Beamforming, and Power Control," *IEEE J. Sel. Areas Commun.*, vol. 38, no. 9, pp. 2057–2073, 2020, doi: 10.1109/JSAC.2020.3000879.
[30] L. L. Mendes *et al.*, "Enhanced Remote Areas Communications: The Missing Scenario for 5G and beyond 5G Networks," *IEEE Access*, vol. 8, pp. 219859–219880, 2020, doi: 10.1109/ACCESS.2020.3042437.
[31] M. A. Salas-Natera, G. L. MacEin, and R. M. Rodriguez-Osorio, "On the design of HAPs High Throughput and flexible 5G Communication Payloads," *2022 16th Eur. Conf. Antennas Propagation, EuCAP 2022*, 2022, doi: 10.23919/eucap53622.2022.9769360.
[32] G. Jang and J. P. Choi, "HAPS Altitude Optimization for Downlink Communications: Alleviating the Effect of Channel Elevation Angles," *IEEE Trans. Aerosp. Electron. Syst.*, vol. PP, pp. 1–11, 2025, doi: 10.1109/TAES.2025.3557774.
[33] R. J. Wang, C. H. Wang, D. N. Yang, G. S. Lee, W. T. Chen, and J. P. Sheu, "Optimizing Resource Block Allocation for Multicast in Beyond 5G Networks," *IEEE Trans. Mob. Comput.*, vol. PP, no. Xx, pp. 1–18, 2025, doi: 10.1109/TMC.2025.3549590.
[34] F. N. Pavlidou, M. Ruggieri, M. Gerla, and R. Miura, "Communications via high altitude platforms: Technologies and trials," *Int. J. Wirel. Inf. Networks*, vol. 13, no. 1, pp. 1–4, 2006, doi: 10.1007/s10776-005-0019-5.
[35] Iskandar and S. Shimamoto, "Analysis of CDMA capacity for multiple stratospheric platform mobile communications under imperfect power control and fading," *IEEE Wirel. Commun. Netw. Conf. WCNC*, no. 1, pp. 2514–2518, 2007, doi: 10.1109/WCNC.2007.468.
[36] TSGR, "Physical channels and modulation (3GPP TS 38.211 version 18.4.0 Release 18)," 2024.
[37] ETSI, "TS 138 104 (V16.4.0) 5G; NR; Base Station (BS) radio transmission and reception," 2020.

Dwi Harinitha received the B.S. degree in Telecommunication Engineering from Telkom University, Bandung, Indonesia, in 2003, and the M.S. degree in Electrical Engineering (Telecommunication) from Institut Teknologi Bandung (ITB), Bandung, Indonesia, in 2010. She is currently pursuing a doctoral's degree at the School of Electrical Engineering and Informatics, ITB.

Iskandar completed his B.E. and M.E. degrees in Telecommunication Engineering from the Institute of Technology Bandung (ITB), Indonesia, in 1995 and 2000, respectively. He received the Doctor Degree from Waseda University, Japan, in 2007. From August 1995 to March 1997, he joined the private telecommunication company that served as a satellite engineer. Since April 1997, he was an Assistant Professor in the Institute of Technology Bandung (ITB). His main fields of research interest are wireless mobile communications and non-terrestrial network communications, which include satellite communications and high-altitude platform (HAPS) communications. Dr. Iskandar is a member of IEEE and has contributed to numerous high-impact journals and conferences in the field of channel propagation, multi-carrier communications, signal processing, and multiple access schemes. Currently, he has been an Associate Professor in the School of Electrical Engineering and Informatics of ITB, Indonesia.

Irma Zakia received the B.E. and Ph.D. degrees in electrial engineering from Institut Teknologi Bandung (ITB), Indonesia, in 2002 and 2014, respectively, and the M.Sc. degree in communications engineering from RWTH Aachen, Germany, in 2007. She is currently an Associate Professor at the School of Electrical Engineering and Informatics ITB. Her research interests centered around massive MIMO systems, optimization theory for communications, high-mobility wireless communications, radar signal processing, and HAPs communications.